RSC Advances

PAPER

View Article Online
View Journal | View Issue

Cite this: *RSC Adv.*, 2022, **12**, 26211

Cold atmospheric plasma driven self-assembly in serum proteins: insights into the protein aggregation to biomaterials†

Rakesh Ruchel Khanikar,‡[a] Parismita Kalita,‡[a] Monika Narzary,‡[a] Deepjyoti Basumatary,[a] Ashim Jyoti Bharati,[a] Anurag Priyadarshi,[b] R. Swaminathan,[b] Heremba Bailung[a] and Kamatchi Sankaranarayanan *[a]

The self-assembly of proteins is crucial in many biomedical applications. This work deals with understanding the role of cold atmospheric plasma (CAP) on the self-assembly of two different proteins present in the serum – BSA and hemoglobin and to elucidate the process associated with the direct application of physical plasma on or in the human (or animal) body, which has implications in therapeutics. The work has been corroborated by several spectroscopic studies such as fluorescence spectroscopy, circular dichroism spectroscopy, and SEM analysis. Through steady-state fluorescence spectroscopy and by following the tryptophan fluorescence, we observed that the emission intensity was quenched for the protein when treated with plasma radiation. Circular dichroism spectroscopy revealed that the structure of the protein was altered both in the case of BSA and hemoglobin. *N*-Acetyl tryptophanamide (NATA), which resembles the tryptophan in the protein, was treated with CAP and we observed the similar quenching of fluorescence as in the proteins, indicating that the protein underwent self-assembly. Time-resolved fluorescence spectroscopy with a decrease in the lifetime revealed that the protein self-assembly was promoted with CAP treatment, which was also substantiated by SEM micrographs. The ROS/RNS produced in the CAP has been correlated with the protein self-assembly. This work will help to design protein self-assembled systems, and in the future, may bring possibilities of creating novel biomaterials with the help of plasma radiation.

Received 13th July 2022
Accepted 31st August 2022

DOI: 10.1039/d2ra04318a

rsc.li/rsc-advances

1. Introduction

Cold atmospheric pressure (CAP) plasma has received a lot of attention in recent years due to its various potential applications in different technologies, such as plasma processing of materials, thin-film deposition, surface modification, plasma medicine and plasma-biomaterial interactions.[1–14] Most (CAP) plasmas for bio-material applications are generated by applying electrical energy to a plasma forming gas (argon, helium, oxygen, nitrogen, air, or mixtures thereof), which further produces hot energetic electrons and low energy ions, resulting in the production of plasma with low temperature.[15–17]

Various research studies use non thermal CAP in biological materials, including cell permeabilization, chronic wound disinfection and healing, decontamination of surfaces, dental applications,[18–21] and the destruction of bacteria, fungi spores and viruses has been reported in the literature.[22–26] In Germany, CAP has been used in trial therapy for head and neck cancer patients.[27,28] Low temperature plasmas have the ability to kill cancer cells without harming healthy ones, leading to the field of plasma oncology.[29–33] The effect of different CAP on proteins such as myoglobin, serum albumin, lysozyme and DNA has been reported.[34–40] Xu *et al.* reported that high voltage CAP induced aggregation and denaturation of BSA.[41] However, they used reactive gases such as oxygen, nitrogen and their combinations for producing the CAP. Pankaj *et al.* reported the use of CAP for Hb and myoglobin, using argon, nitrogen and air as plasma-forming gas, and have shown that the structural modifications of the proteins occur.[42]

Therefore, there is a direct need to understand the role of self-assembly of biomolecules such as proteins, lipids and DNA when subjected to different gas-fed CAP to bring out a more complete understanding of plasma medicine. In this regard, through this work we report the effect of helium plasma on two major proteins in the blood serum, albumin and hemoglobin. We have evaluated the structural changes of these two proteins as it is primarily important for carrying out their respective

[a]*Biophysics – Physical Sciences Division, Institute of Advanced Study in Science and Technology, (An Autonomous Institute Under DST, Govt. of India), Vigyan Path, Paschim Boragaon, Garchuk, Guwahati, Assam 781035, India. E-mail: kamatchi.sankaran@gmail.com*

[b]*Department of Biosciences and Bioengineering, Indian Institute of Technology Guwahati, Guwahati 781039, Assam, India*

† Electronic supplementary information (ESI) available. See https://doi.org/10.1039/d2ra04318a

‡ Contributed equally.

functions. The effect of cold atmospheric plasma on these two proteins BSA and hemoglobin has been studied as a function of the time of treatment of the proteins. We evaluated the self-assembly of these proteins with plasma irradiation for 1, 3, 5, 7, and 10 min. The effective changes in the structure of the protein were substantiated using various spectroscopic techniques and microscopic techniques. We observed that the self-assembly was promoted in respect to the He plasma, and this model could be useful in building prototypes for wound healing.

2. Experimental methods

2.1 Materials

Proteins BSA and hemoglobin, and *N*-acetyl tryptophanamide were purchased from Sigma with 99% purity, and was used as such. The protein solutions were prepared at a concentration of 1 μM for all of the measurements. Millipore water was used for the preparation of the buffer, and all the protein solutions were made in phosphate buffer pH 7.5.

Experimental setup. In this experiment, a novel four-jet CAP plasma array was developed indigenously to treat the protein samples, as shown in Fig. 1. The four-jet structure helped us achieve a higher plasma dose than the single jet plasma used in our earlier works for the same treatment time.[26,51] It consisted of four dielectric tubes made of glass with an inner diameter of 5 mm and an outer diameter of 7 mm fitted into a Teflon housing with a gas inlet, as shown in the figure. On the outer surface of the glass tubes, aluminium strips of width 7 mm were wrapped around near the end and connected together, which served as the powered electrode. A stainless-steel sheet placed below the Petri dish containing the sample was used as the grounded electrode. Helium was used as the plasma forming gas. A gas flow rate of 2–4 slm (standard litre per minute) was maintained to obtain a stable plasma. The gas flow was measured using a variable area flowmeter (Cole Palmer). The plasma produced in the glass tubes came out into the open air with the gas flow. A high voltage sinusoidal power supply (Ionics Power Solutions Pvt. Ltd.) was used to power the device. A high voltage of 4 kV at a frequency 30 kHz was applied to produce the plasma. The sample was then irradiated for different exposure times.

The various reactive species present in the plasma were then investigated by obtaining an emission spectrum of the plasma using an optical emission spectrometer (Andor-SR-303i-A). The light emitted from the plasma was collected by an optical fiber fitted to the spectrometer equipped with three gratings consisting of 300, 1200 and 2400 grooves per mm, and the slit width was varied from 10–2500 μm. In this experiment, a slit width of 50 μm was used to achieve a fair resolution along with sufficient intensity. The survey spectrum was recorded using 1200 grooves per mm grating in the wavelength range of 300–900 nm, whereas the OH emission was recorded using 2400 grooves per mm grating in the wavelength range of 306–310 nm to achieve high resolution. The spectrometer was calibrated using a standard NIST traceable calibration lamp (StellarNet Inc.).

2.2 UV-vis and fluorescence spectroscopy

The samples were analysed using a UV-1800-Shimadzu spectrophotometer with quartz cells of 1 cm path length with the corresponding buffer as reference for the measurements. The steady state fluorescence spectroscopy measurements were performed using a Cary Eclipse Spectrometer with $\lambda_{ex} = 280$ nm.

2.3 CD spectroscopy

The CD spectra of the pure protein at pH 7.5 and after treatment with plasma radiation were obtained using a JASCO J-715 spectropolarimeter (JASCO Corp., Tokyo). The far-UV (240–190 nm) spectra of the protein in different time treatments with plasma were obtained using 0.1 cm path length quartz cells. All measurements were done a minimum of three times to ensure reproducibility.

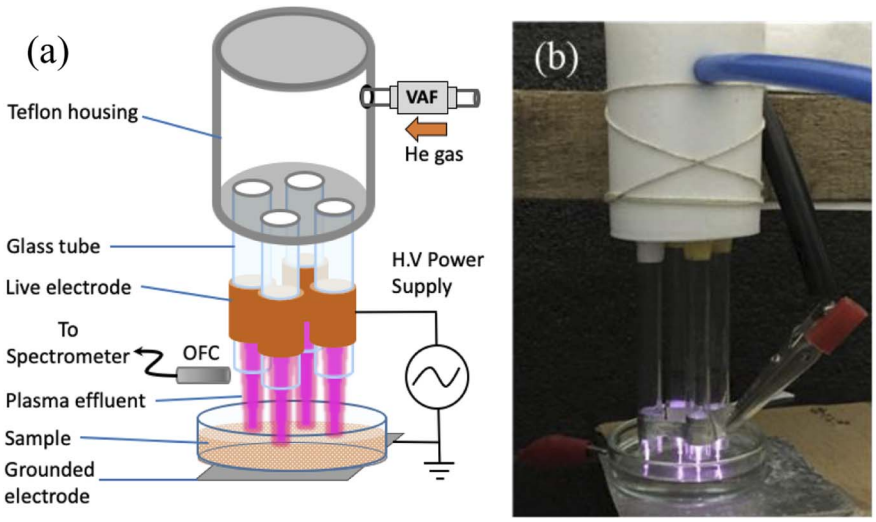

Fig. 1 (a) Schematic of the experimental setup. OFC: optical fiber cable, VAF: variable area flowmeter. (b) Photograph of the plasma generated.

2.4 Time-resolved fluorescence decay

Time-resolved fluorescence intensity decay measurements were performed using a time-correlated single photon counting (TCSPC) instrument equipped with a motorized polarizer (Make: Horiba Scientific). A 295 nm Deltadiode pulsed light source with a 20 MHz repetition rate and ~0.8 ns instrument response function FWHM was used to excite the samples. A photomultiplier tube (PPD-900, Horiba Scientific) and a band-pass filter (KV370) were used to acquire the signals.[43] To avoid contribution from anisotropy decay, the fluorescence decays were collected at magic angle settings (54.7°). NATA was used as a standard to verify the performance of the instrument before measuring the lifetime of the samples. The absorbance of the samples at the excitation wavelength were kept to less than 0.09 to avoid inner filter effects. A chalk powder suspension was used to measure the IRF. A total of 15 000 counts was recorded for the decays and three independent measurements were performed. The intensity decays were collected in a 1 cm path length quartz cuvette. Discrete exponential analysis of the collected fluorescence intensity decays was performed using the method of non-linear least squares to obtain the mean lifetime and fit parameters.[44]

2.5 Microscopy

Secondary electron microscopy was used to study the morphology of the films of protein transferred to solid surfaces. The protein solution was allowed to reach the equilibrium surface tension. The films were then transferred onto cleaned solid substrates using the Langmuir–Schaefer film transfer technique and characterized using scanning electron microscopy (SEM). A thin layer of gold (200 Å) was sputtered on these samples, and SEM studies were undertaken using a Hitachi S4800 model.

2.6 Zeta potential and dynamic light scattering (DLS) measurements

Zeta potential and DLS studies were carried out using a Malvern Zetasizer Nanoseries, Nano-ZS90. The measurements of the average particle size and ζ-potential of the aqueous suspensions of amelogenin were carried out on a Malvern Zetasizer Nano-ZS dynamic light-scattering (DLS) analyzer (Malvern Instruments Ltd., Malvern, Worcestershire, UK). Samples (n > 3 for each protein, including various batches) of 1 mL were analysed for particle size and ζ-potential in multiple runs with increasing pH, with approximately 2 h required to cover the examined pH range. Each datum was the result of averaging over 100 acquisitions, each lasting about 10 s. The particle sizes reported present the hydrodynamic diameters derived from the time-correlation function of the particle number density.

2.7 DNPH assay

The carbonyl content of the untreated and plasma treated protein samples was determined by 2,4-dinitrophenylhydrazine (DNPH) assay.[45] Briefly, 200 μL protein samples were properly mixed with 800 μL of freshly prepared 0.1% 2,4-dinitrophenylhydrazine in 2.5 M HCl, and incubated for 1.5 h at room temperature. The protein was precipitated by the addition of 1000 μL of 20% chilled trichloroacetic acid (TCA), followed by centrifugation at 4 °C. The pellet was then re-suspended and washed with chilled 10% TCA, followed by washing twice with ice-cooled 50 : 50 (v/v) acetate and ethanol. Finally, the pellet was re-suspended in 500 μL of 6 M guanidium chloride and the absorption spectra were recorded at 370 nm.

3. Results and discussion

The plasma glow was recorded using an optical emission spectrometer, which exhibited various plasma-generated reactive species. Fig. 2 presents the emission spectrum, which mainly consists of excited neutral He atoms (He I). In addition, molecular bands such as OH (A–X), N_2 (C–B), N_2^+ (B–X), atomic hydrogen (H) line and excited atomic oxygen (O) lines were observed in the spectrum. The spectral lines were identified with the help of the NIST atomic spectra database[46] and other literature.[47] The reactive species in the plasma are known to be produced by electron impact phenomena, which cause ionization, excitation and dissociation of the molecules. These plasma-generated reactive species diffuse into the liquid media, thereby forming reactive oxygen and nitrogen species (RONS) in the sample solution.[48] Interaction of high energetic electrons with the liquid surface dissociates water molecules, which might be responsible for forming O and H-related reactive radicals. These reactive species are highly favourable to react with air molecules, which gives rise to the formation of nitrogen reactive species (RON) (*e.g.*, N_2^+, NO). These N-related species are highly unstable and interact with the O to form nitrate/nitrite (NO_2^-, NO_3^-). The He plasma is suitable for biomedical applications because of its low gas temperature value. The gas temperature was estimated by comparing the experimental spectrum with a theoretically simulated spectrum provided by software like LIFBASE[49] and SPECAIR,[50] as described in our previous publications.[26,51] The temperature of the plasma jet array was found to be ~310 K in the plasma region. As a result of

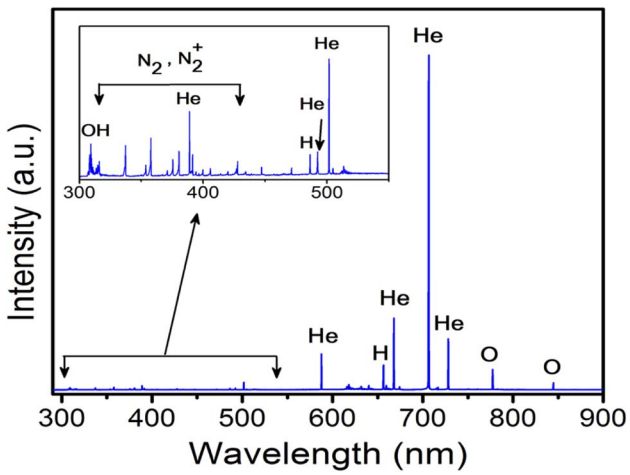

Fig. 2 OES spectra of the He gas fed plasma jet.

this low plasma temperature, the sample also remained at room temperature after plasma treatment. It is very complex to understand this plasma zone and the individual role of the reactive species during treatment.

The BSA and Hb samples were treated with CAP jet (Fig. 1) for different time intervals (t – 1, 3, 5, 7, 10 min). BSA has 2 tryptophan residues and hemoglobin consists of 6 tryptophan residues in its structure along with 4 heme (porphyrin) groups, and thus make the protein bulkier. UV-visible spectra (Fig. S1(a) and (b)†) of the BSA and Hb protein peaks centered around 280 nm arose due to the tryptophan residue in the protein, and in the case of Hb, another peak at 410 nm arose due to the Soret band.[52]

Fig. 3(a) shows the intrinsic fluorescence intensity of BSA before and after treatment with plasma. The intrinsic fluorescence of native BSA is dominated by tryptophan (Trp) emission for an excitation wavelength at 280 nm. BSA has two Trp residues, Trp-134 in the first domain and Trp-213 in the second domain, which are in quite different environments. Trp-213 is located in a hydrophobic binding pocket and Trp-134 is on the surface of the molecule.[53] The emission maxima wavelength (λ_{max}) does not change for the native protein and for the plasma treated protein. The absence of the emission maximum shift indicates the absence of significant changes in the conformation around either Trp residues. At the same time, we observed a quenching in the fluorescence. The quenching of the fluorescence intensity can be mainly due to the tryptophan accessibility. Hence, after the plasma treatment, there could be structural re-ordering in the protein.

Fig. 3(b) and (c) show the steady state fluorescence spectra for Hb for λ_{ex} at 280 nm and 409 nm, respectively. We observed a quenching of the fluorescence when the protein was excited at λ_{ex} 280 nm. On the other hand, Fig. 3(c) shows the Soret band dynamics of the protein at λ_{ex} 409 nm, where the changes in the protein structure upon plasma treatment around the heme groups led to an increase in the emission intensity. This may be due to the self-assembly of the protein and the heme groups being stacked next to each other. Quenching in the tryptophan fluorescence is generally attributed to the addition of the electron-rich species. Hence, the plasma treatment has led to the quenching due to the interaction of the proteins with the highly electron rich plasma.[54]

To verify the conformational changes in the protein, circular dichroism spectroscopy was performed for the BSA and Hb

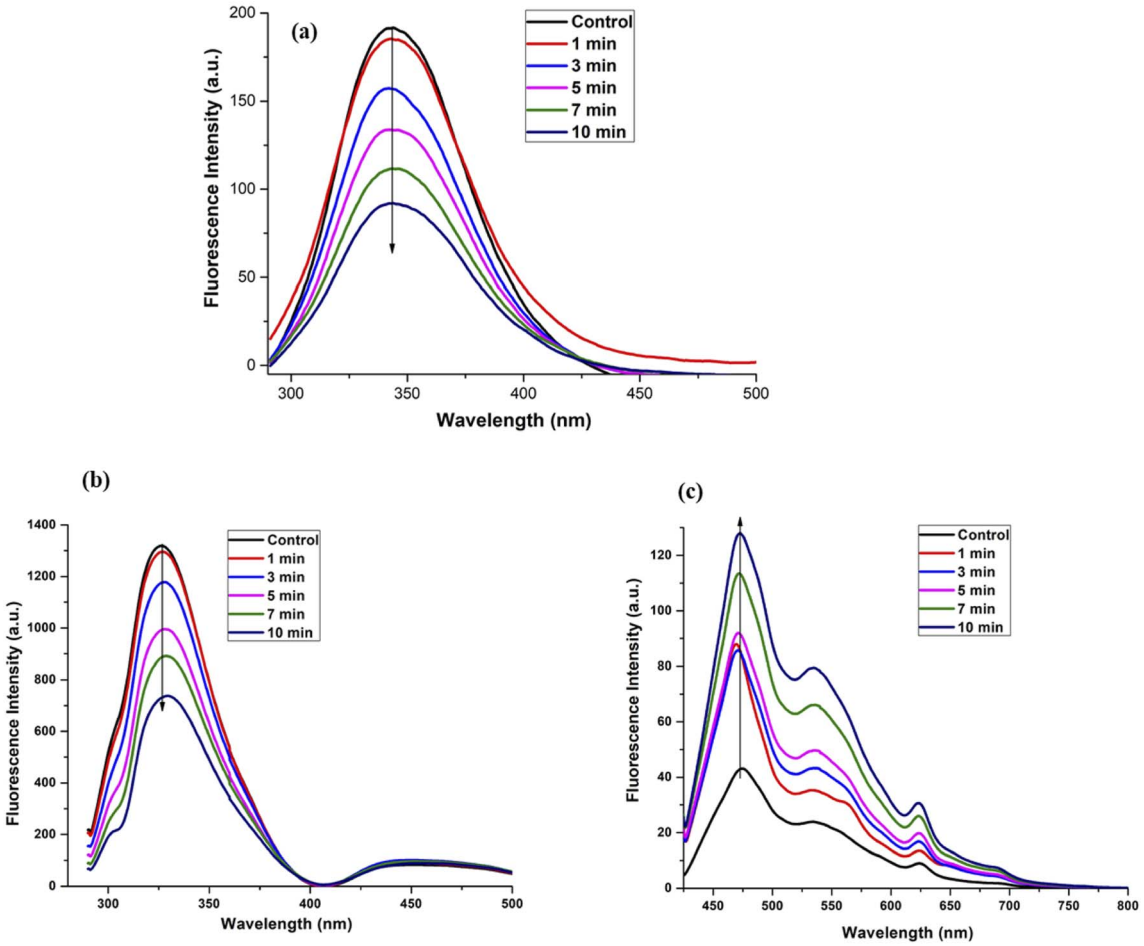

Fig. 3 Fluorescence spectroscopy of control and plasma treated (a) BSA with λ_{ex} = 280 nm, (b) Hb with λ_{ex} = 280 nm, and (c) Hb with λ_{ex} = 409 nm.

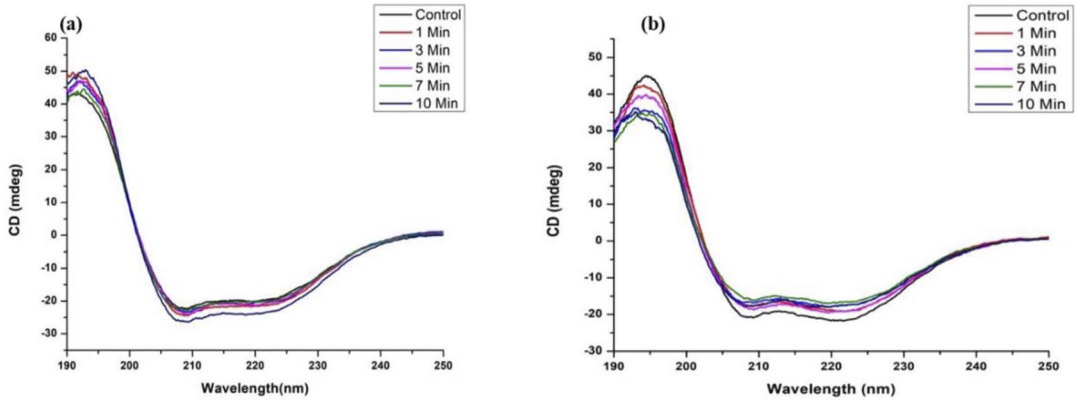

Fig. 4 CD spectra of control and plasma treated (a) BSA and (b) Hb.

samples. Fig. 4 shows the native protein with the minima around 208 nm and 222 nm corresponding to the α-helical structure. The native protein was seen to be intact even after plasma treatment for 10 min for both proteins, which is in accordance with the fluorescence measurements.

To clearly understand the quenching of the protein fluorescence after plasma treatment and to verify the role of tryptophan in the proteins, we performed steady-state measurements on the molecule *N*-acetyl tryptophanamide (NATA), which resembles the tryptophan in the protein. Fig. 5(a) shows the structure of the NATA, and Fig. 5(b) shows the fluorescence emission graph of NATA after treatment with plasma radiation. We observed a similar quenching of fluorescence of the native molecule, which is very similar to the protein environment. Thus, we ascertained that the transitions occurring in the protein are due to the conformational changes around the tryptophan.

To further probe the dynamics of the excited state fluorophore in the proteins, picosecond fluorescence lifetime spectroscopy was carried out and is presented in Fig. 6 for BSA and Hb. Additionally, we performed the picosecond lifetime spectra of NATA, and are presented in the supplementary section. Fig. S2–S4† presents the emission spectra, and Tables S1–S3† represent the calculated lifetime for BSA, Hb and NATA, respectively. In the case of BSA, as there are two Trp in the protein. We observed a bi-exponential decay with a lifetime of the control sample to be 2.17 ns and 6.22 ns. Trp-213 is located in a hydrophobic binding pocket and Trp-134 is on the surface of molecule (Fig. S5(a)†). Hence, the shorter lifetime may be attributed to the Trp-213 in the hydrophobic core and Trp-134 with the longer lifetime. Such changes in the lifetime due to the presence of the Trp in the different locations in an enzyme have been reported earlier.[55] However, an increase in the plasma treatment time to 10 min leads to a slight decrease in the lifetime to 2.05 ns and 6.06 ns, together with a shift in the % population of the species. It clearly indicates that the protein undergoes a self-assembly with the plasma treatment time. This may be due to the fact that the CAP-treated protein samples, due to self-assembly, cannot reach the higher energy level similar to the control samples. Hence, the decay time may be faster. The decay times decrease from 0.42 ns to 0.28 ns for τ_1 together with an increase in the % population, clearly indicating that the protein undergoes a self-assembly process as in the case of BSA. Such changes in the lifetime and the protein self-assembly have been previously reported.[56] In the case of Hb, we observed a tri-exponential decay since the protein has six tryptophan residues and four heme (porphyrin) groups (Fig. S5(b)†). Reports show that the hemoglobin has six tryptophan residues (α14, β15 and

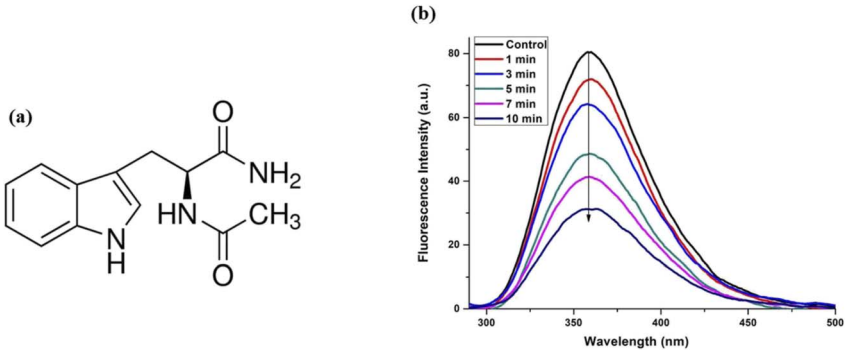

Fig. 5 (a) Structure and (b) fluorescence spectra of NATA after plasma treatment.

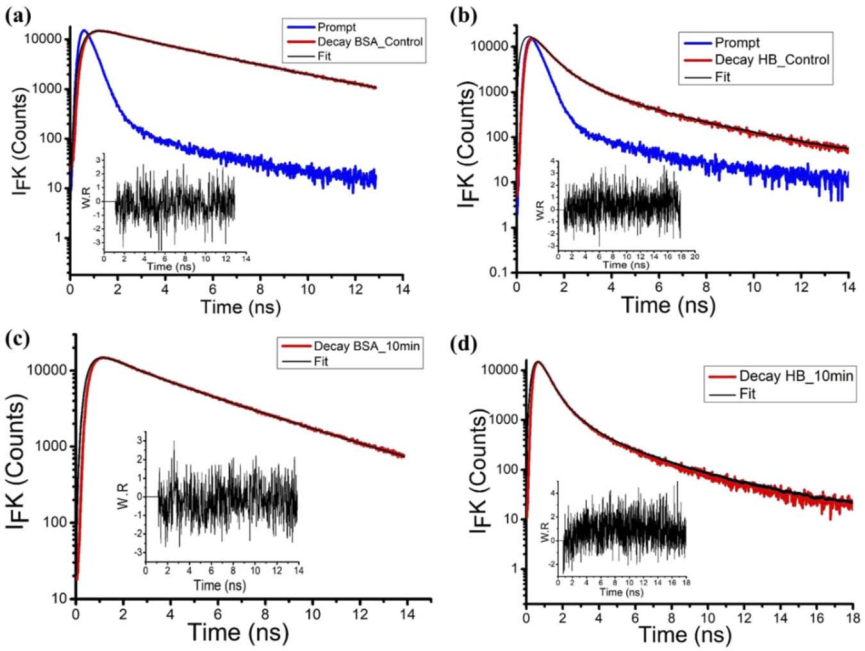

Fig. 6 Time-resolved fluorescence spectroscopy of the proteins (a) and (c) BSA and (b) and (d) Hb after CAP treatment.

β37 in each dimer). However, only the two tryptophan residues (β37 of each subunit) positioned in the hydrophobic core are principally responsible for its intrinsic fluorescence (Hirsch *et al.*, 1980; Hirsch & Nagel, 1981). Hence the tri-exponential decay can be attributed to these two Trp in the β37 subunits, and the longer decay time is attributed to the heme group. The changes in the τ_1, τ_2 and τ_3, along with the % population clearly show that the protein undergoes self-assembly. On the contrary, it can be clearly seen that the lifetime of control NATA (Table S3†) is around 3.15 ns, and it remains almost the same with the plasma treatment. This indicates that only the proteins could undergo the self-assembly.

To understand the effect of oxidative stress induced due to the CAP treatment on the proteins, arising due to the reactive species present in the plasma, the 2,4-dinitrophenylhydrazine (DNPH) assay was carried out and is presented in Fig. 7. It can be noted that the protein BSA undergoes a higher oxidative stress due to the plasma treatment for 10 minutes, whereas the protein Hb does not drastically change. This small change could be due to the presence of heavy heme groups in the protein, taking up the highly charged electrons from the plasma. However, we also observed that there is no change in the charge on both proteins, and both maintained similar zeta potentials (Table 1) as the controls.

SEM micrographs of the samples revealed that after the protein undergoes the CAP treatment, morphological transitions occur (Fig. 8). However, the CD analysis shows that there are minimal changes in the secondary structure. This further confirms that both BSA and Hb proteins undergo self-assembly with the plasma treatment, which can be very useful in the biomedical applications.

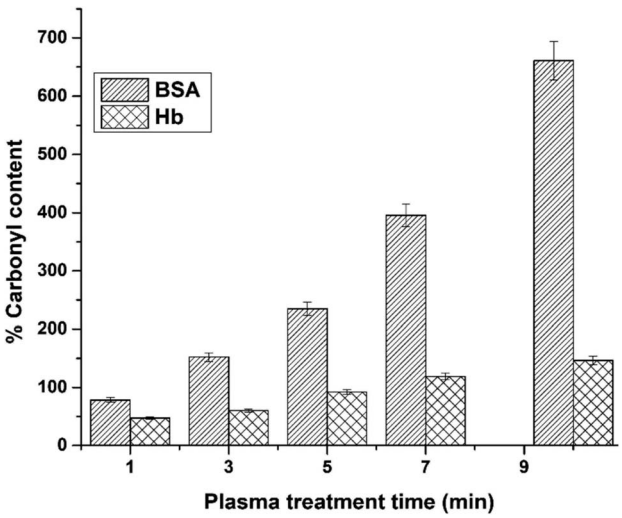

Fig. 7 Relative change in the % carbonyl content in BSA and Hb protein after CAP treatment time with reference to the control using the DNPH assay.

Table 1 Zeta potential of the protein samples after CAP treatment

Sample	BSA	Hb
0 minute	−10.4	−4.80
1 minute	−11.5	−6.90
3 minute	−10.83	−6.60
5 minute	−10.4	−6.33
7 minute	−11.38	−6.98
10 minute	−11.5	−6.63

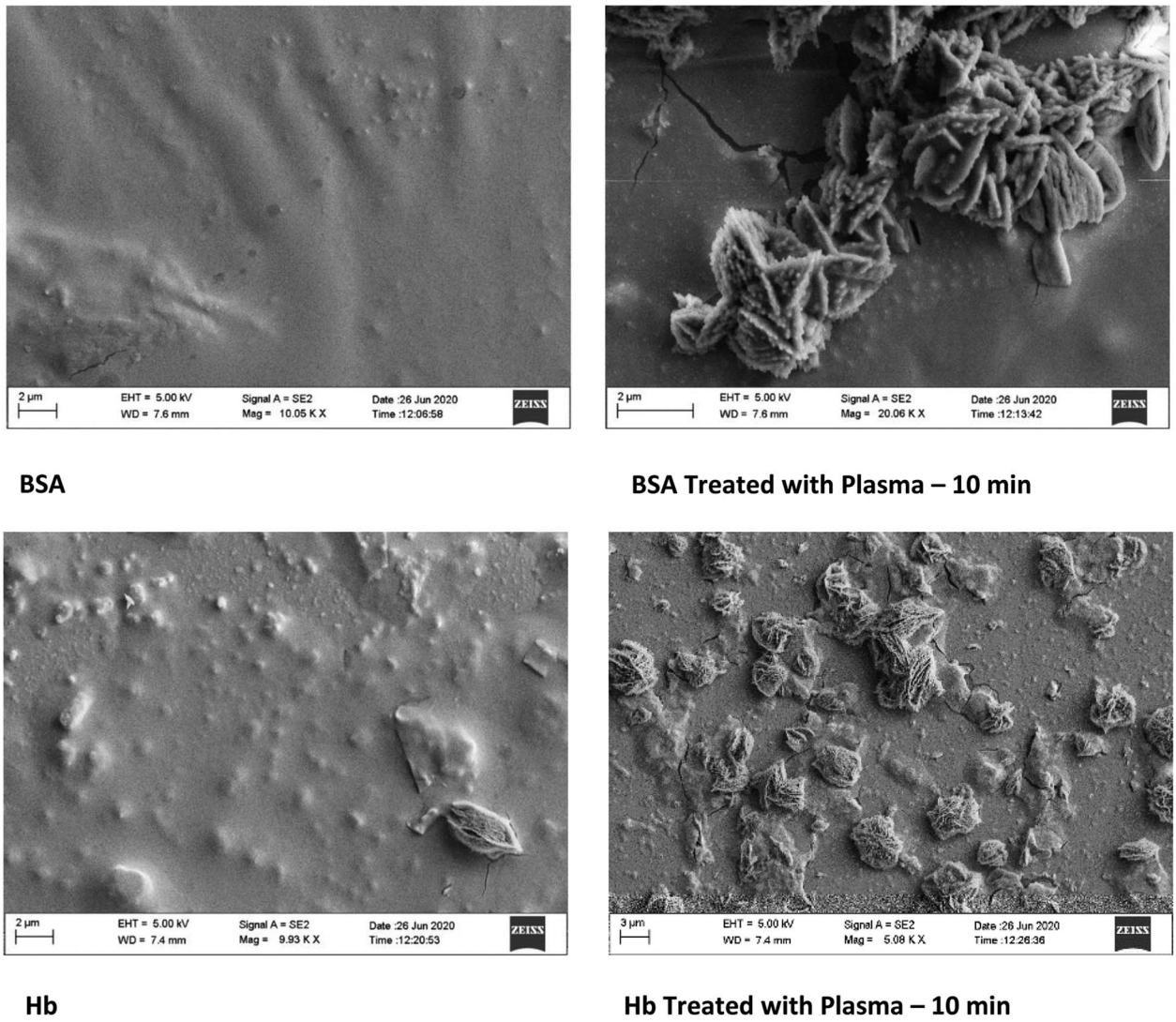

Fig. 8 SEM micrographs of BSA and Hb before and after CAP treatment.

Reactive oxygen/nitrogen species are an integral part of the CAP and interact with the proteins, causing further reactions in the solution. To elucidate the protein self-assembly due to CAP treatment, we studied the different ROS/RNS associated with the CAP treatment using the protocols mentioned in the literature[26] and given in Table 2.

It should be noted that the presence of OH and H_2O_2 decreases with increased CAP treatment. However, the nitrates NO_3 and NO_2 increase. The increase in the nitrates may have a significant role in the self-assembly of the proteins, and such studies have been previously reported in the literature.[57,58]

Table 2 ROS/RNS species present in the plasma for different exposure times

Time (min)	OH radicals	H_2O_2	NO_3	NO_2
5	14.7 ± 0.9	37.82 ± 1.1	4.35 ± 0.4	5.39 ± 0.9
10	12.9 ± 0.24	30.41 ± 0.7	5.53 ± 0.3	6.27 ± 0.1

4. Conclusions

In this work, we have evaluated the effect of CAP with He as the plasma-forming gas on two proteins, bovine serum albumin and hemoglobin, which are relevant in the wound healing process. We have seen that the proteins undergo macromolecular self-assembly with intact secondary structural features, as evidenced by various biophysical techniques, including fluorescence lifetime measurements and SEM analysis. Earlier reports showed that serum proteins underwent denaturation upon CAP treatment. In our work, we have demonstrated that the tuning of ROS/RNS using a suitable plasma-forming gas will help in the process of achieving protein self-assembly without denaturing the proteins. These results give an outlook for the utilization of cold atmospheric plasma for biomedical applications, especially in treating infections that occur during the wound healing process, as directed protein self-assembly is essential in this process.

Conflicts of interest

The authors declare no conflicts to declare.

Acknowledgements

K. S. thanks DST-IASST, Guwahati for the in-house project grant and SERB, Govt. of India for the SRG grant (SRG/2020/001894 dt. 11.11.2020). R. R. K. thanks DST, Govt. of India for the support under DST-INSPIRE Fellowship Scheme. P. K. and D. B. would like to thank DST, Govt. of India and IASST for the research fellowship. The authors thank SAIC, IASST for the analytical facilities. The authors thank the Department of Biosciences and Bioengineering, IIT Guwahati for the Time-Resolved (TCSPC) fluorescence spectrophotometer facility.

References

1 S. Q. Xiao, S. Xu and K. Ostrikov, *Mater. Sci. Eng., R*, 2014, **78**, 1–29.
2 R. A. Jelil, *J. Mater. Sci.*, 2015, **50**, 5913–5943.
3 H. Kakiuchi, H. Ohmi and K. Yasutake, *J. Vac. Sci. Technol., A*, 2014, **32**, 030801.
4 M. Moravej and R. F. Hicks, *Chem. Vap. Deposition*, 2005, **11**, 469–476.
5 A. B. Gil'Man, *High Energy Chem.*, 2003, **37**, 17–23.
6 M. S. Kang, B. Chun and S. S Kim, *J. Appl. Polym. Sci.*, 2001, **81**, 1555–1566.
7 H. Drnovská, L. Lapčík, V. Buršíková, J. Zemek and A. M. Barros-Timmons, *Colloid Polym. Sci.*, 2003, **281**, 1025–1033.
8 M. Laroussi, *IEEE Trans. Plasma Sci.*, 2015, **43**, 703–712.
9 S. Mohades, N. Barekzi and M. Laroussi, *Plasma Processes Polym.*, 2014, **11**, 1150–1155.
10 K. Miyamoto, S. Ikehara, H. Takei, Y. Akimoto, H. Sakakita, K. Ishikawa, M. Ueda, J. I. Ikeda, M. Yamagishi, J. Kim and T. Yamaguchi, *Arch. Biochem. Biophys.*, 2016, **605**, 95–101.
11 K. Miyamoto, S. Ikehara, H. Sakakita and Y. Ikehara, *J. Clin. Biochem. Nutr.*, 2017, **60**, 25–28.
12 I. Levchenko, M. Keidar, U. Cvelbar, D. Mariotti, A. Mai-Prochnow, J. Fang and K. K Ostrikov, *J. Phys. D: Appl. Phys.*, 2016, **49**, 273001.
13 F. Poncin-Epaillard and G. Legeay, *J. Biomater. Sci., Polym. Ed.*, 2003, **14**, 1005–1028.
14 T. Desmet, R. Morent, N. De Geyter, C. Leys, E. Schacht and P. Dubruel, *Biomacromolecules*, 2009, **10**, 2351–2378.
15 A. Schutze, J. Y. Jeong, S. E. Babayan, J. Park, G. S. Selwyn and R. F. Hicks, *IEEE Trans. Plasma Sci.*, 1998, **26**, 1685–1694.
16 H. Conrads and M. Schmidt, *Plasma Sources Sci. Technol.*, 2000, **9**, 441.
17 A. P. Napartovich, *Plasmas Polym.*, 2001, **6**, 1–4.
18 M. Leduc, D. Guay, R. L. Leask and S. Coulombe, *New J. Phys.*, 2009, **11**, 115021.
19 G. Isbary, W. Stolz, T. Shimizu, R. Monetti, W. Bunk, H. U. Schmidt, G. E. Morfill, T. G. Klämpfl, B. Steffes, H. M. Thomas, J. Heinlin, S. Karrer, M. Landthaler and J. L. Zimmermann, *Clin. Plasma Med.*, 2013, **1**, 25–30.
20 M. Korachi and N. Aslan, *Microbial pathogens and strategies for combating them: science, technology and education*, 2013, vol. 1, pp. 453–459.
21 S. Cha and Y. S. Park, *Clin. Plasma Med.*, 2014, **2**, 4–10.
22 M. Moreau, N. Orange and M. G. Feuilloley, *Biotechnol. Adv.*, 2008, **26**, 610–617.
23 O. Lunov, O. Churpita, V. Zablotskii, I. G. Deyneka, I. K. Meshkovskii, A. Jäger, E. Syková, Š. Kubinová and A. Dejneka, *Appl. Phys. Lett.*, 2015, **106**, 053703.
24 P. Puligundla and C. Mok, *World J. Microbiol. Biotechnol.*, 2018, **34**, 1–2.
25 A. Filipić, I. Gutierrez-Aguirre, G. Primc, M. Mozetič and D. Dobnik, *Trends Biotechnol.*, 2020, **38**, 1278–1291.
26 R. R Khanikar, M. Kalita, P. Kalita, B. Kashyap, S. Das, M. R. Khan, H. Bailung and K. Sankaranarayanan, *RSC Adv.*, 2022, **12**, 9466–9472.
27 H. R. Metelmann, D. S. Nedrelow, C. Seebauer, M. Schuster, T. V. Woedtke, K. D. Weltmann, S. Kindler, P. H. Metelmann, S. E. Finkelstein, D. D. V. Hoff and F. Podmelle, *Clin. Plasma Med.*, 2015, **3**, 17–23.
28 R. Rutkowski, M. Schuster, J. Unger, C. Seebauer, H. R. Metelmann, T. V. Woedtke, K. D. Weltmann and G. Daeschlein, *Clin. Plasma Med.*, 2017, **7**, 52–57.
29 X. Dai, K. Bazaka, D. J. Richard, E. R. Thompson and K. K. Ostrikov, *Trends Biotechnol.*, 2018, **36**, 1183–1198.
30 M. Keidar, *Plasma Sources Sci. Technol.*, 2015, **24**, 033001.
31 M. Wang, B. Holmes, X. Cheng, W. Zhu, M. Keidar and L. G. Zhang, *PLoS One*, 2013, **8**, 73741.
32 A. Azzariti, R. M. Iacobazzi, R. D. Fonte, L. Porcelli, R. Gristina, P. Favia, F. Fracassi, I. Trizio, N. Silvestris, G. Guida and S. Tommasi, *Sci. Rep.*, 2019, **9**, 1–3.
33 S. Mitra, L. N. Nguyen, M. Akter, G. Park, E. H. Choi and N. K. Kaushik, *Cancers*, 2019, **11**, 1030.
34 J. H. Park, M. Kim, M. Shiratani, A. Cho, E. H. Choi and P. Attri, *Sci. Rep.*, 2016, **6**, 1–4.
35 P. Attri, M. Kim, T. Sarinont, E. H. Choi, H. Seo, A. E. Cho, K. Koga and M. Shiratani, *Sci. Rep.*, 2017, **7**, 1–3.
36 C. H. Song, P. Attri, S. K. Ku, I. Han, A. Bogaerts and E. H. Choi, *J. Phys. D: Appl. Phys.*, 2021, **54**, 185202.
37 S. Choi, P. Attri, I. Lee, J. Oh, J. H. Yun, J. H. Park, E. H. Choi and W. Lee, *Sci. Rep.*, 2017, **7**, 1–10.
38 H. Lu, S. Patil, K. M. Keener, P. J. Cullen and P. Bourke, *J. Appl. Microbiol.*, 2014, **116**, 784–794.
39 A. Stypczyńska, S. Ptasińska, B. Bahnev, M. Bowden, N. S. Braithwaite and N. J. Mason, *Chem. Phys. Lett.*, 2010, **500**, 313–317.
40 S. B. Park, B. Kim, H. Bae, H. Lee, S. Lee, E. H. Choi and S. J. Kim, *PLoS One*, 2015, **10**, 0129931.
41 L. Xu, H. Hou, B. Farkas, K. M. Keener, A. L. Garner and B. Tao, *LWT*, 2021, **149**, 111995.
42 P. Attri, N. Kumar, J. H. Park, D. K. Yadav, S. Choi, H. S. Uhm, I. T. Kim, E. H. Choi and W. Lee, *Sci. Rep.*, 2015, **5**, 1–2.
43 M. Z. Ansari and R. Swaminathan, *Proteins: Struct., Funct., Bioinf.*, 2020, **88**, 889–909.
44 R. Swaminathan, G. Krishnamoorthy and N. Periasamy, *Biophys. J.*, 1994, **67**, 2013–2023.

45 R. L. Levine, J. A. Williams, E. R. Stadtman and E. Shacter, *Methods Enzymol.*, 1994, **233**, 346–357.
46 A. Kramida, Y. Ralchenko, J. Reader and NIST ASD Team, *NIST Atomic Spectra Database*, version 5.8**https://physics.nist.gov/PhysRefData/ASD/lines_form/**, accessed July 2022.
47 R. W. B. Pearse and A. G. Gaydon, *The Identification of Molecular Spectra*, Chapman & Hall Ltd, London, 2nd edn, 1950.
48 M. Magureanu, D. Piroi, F. Gherendi, N. B. Mandache and V. Parvulescu, *Plasma Chem. Plasma Process.*, 2008, **28**, 677–688.
49 J. M. Luque and D. R. Crosley, LIFBASE: Database and Spectral Simulation Program (Version 2.1), *SRI Int. Rep. MP*, 1999, vol. 99, (009), **https://archive.sri.com/engage/products-solutions/lifbase/**, accessed July 2022.
50 C. O. Laux, Radiation and nonequilibrium collisional–radiative models, *Physico-Chemical Model. High Enthalpy Plasma Flows*, ed. D. Fletcher, von Karman Inst. Spec. Course, Rhode-Saint-Genèse, Belgium, 2002, **http://www.specair-radiation.net/**, accessed July 2022.
51 R. R. Khanikar, P. J. Boruah and H. Bailung, *Plasma Res. Express*, 2020, **2**, 045002.
52 E. Heftmann, *Chromatography: Fundamentals and Applications of Chromatography and Related Differential Migration Methods*, Journal of Chromatography Library, Elsevier, Netherlands, 1991.
53 Y. Moriyama, D. Ohta, K. Hachiya, Y. Mitsui and K. Takeda, *J. Protein Chem.*, 1996, **15**, 265–272.
54 M. F. Pignataro, M. G. Herrera and V. I. Dodero, *Molecules*, 2020, **25**, 4854.
55 B. Campanini, S. Raboni, S. Vaccari, L. Zhang, P. F. Cook, T. L. Hazlett, A. Mozzarelli and S. Bettati, *J. Biol. Chem.*, 2003, **278**, 37511–37519.
56 K. Sankaranarayanan, A. Dhathathreyan, J. Krägel and R. Miller, *J. Phys. Chem. B*, 2012, **116**, 895–902.
57 J. M. Souza, Q. Chen, B. Blanchard-Fillion, S. A. Lorch, C. Hertkorn, R. Lightfoot, M. Weisse, T. Friel, E. Paxinou, M. Themistocleous, S. Chov and H. Ischiropoulos, Reactive nitrogen species and proteins: biological significance and clinical relevance, *Biological Reactive Intermediates VI*, 2001, pp. 169–174.
58 B. Hu, Z. Lian, Z. Zhou, L. Shi and Z. Yu, *ACS Appl. Bio Mater.*, 2020, **3**, 5529–5551.